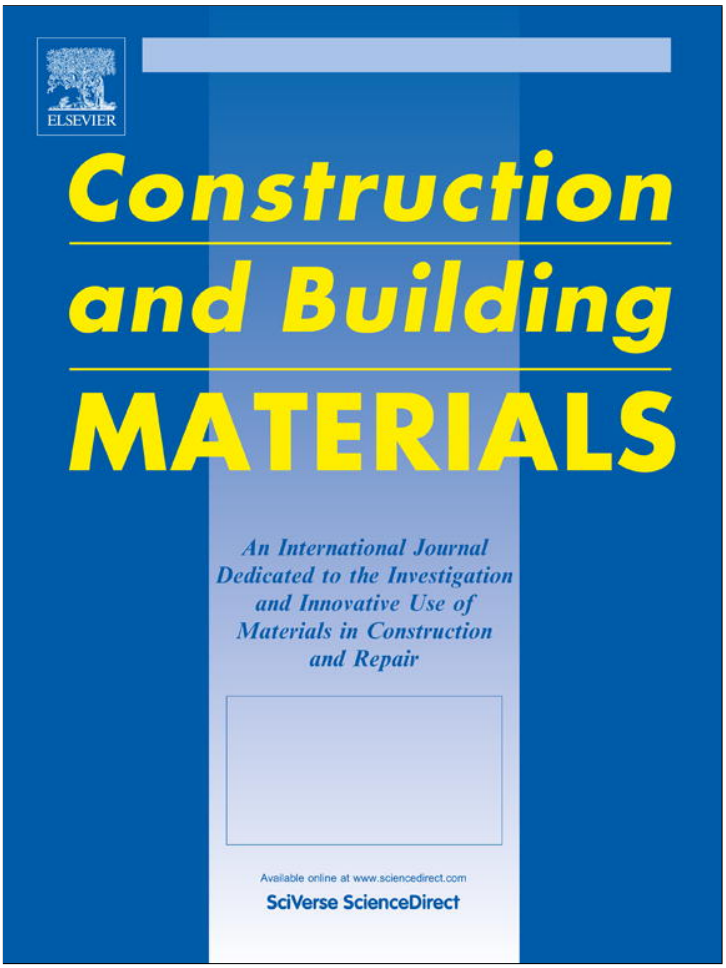

Construction and Building Materials 45 (2013) 282–288

Contents lists available at SciVerse ScienceDirect

Construction and Building Materials

journal homepage: www.elsevier.com/locate/conbuildmat

Crack classification in reinforced concrete beams with varying thicknesses by mean of acoustic emission signal features

M.A.A. Aldahdooh, N. Muhamad Bunnori *

School of Civil Engineering, Universiti Sains Malaysia (USM), Malaysia

HIGHLIGHTS

- We examine the changes in the beam thicknesses about the AE signal features.
- Increasing beam thickness will increase the A-FRQ values.
- Increasing beam thickness will decrease the RA values.
- Increasing the degree of damage will decrease the A-FRQ values.
- Increasing the degree of damage will increase the RA values.

ARTICLE INFO

Article history:
Received 9 January 2013
Received in revised form 22 March 2013
Accepted 22 March 2013

Keywords:
Non-destructive testing
Flexural cracks
Shear cracks
AE parameter analysis-based method
Mix-mode cracks

ABSTRACT

This paper describes an application of the acoustic emission signal features in the structure health monitoring (SHM) fields. The most popular applications of acoustic emission signal in SHM are specified on crack monitoring, quantifying the degree of damage and crack classification. In this study, the acoustic emission signal is applied to classify the types of cracks (flexural or shear cracks) of several types of RC beams subjected to four-point bending. Generally, the two common methods used in crack classification are the AE parameter analysis-based method and the signal-based method. The aim of this study is to classify the crack types of RC beams with varying thicknesses based on the fracture mechanism of the RC beams and the acoustic emission signal features. As a result, the ratio of shear cracks at the failure stage becomes 17.10%, 14.50% and 12.05% of the AE hits for the 20 cm, 25 cm and 30 cm beam thickness, respectively. These results coincided with the visual observation results according to crack modes. The results of the present application can be utilized in health monitoring of vital concrete structures such as bridges, and any RC member subjected to bending load. Which in term is used for prioritization of repair and retrofitting processes for these structures.

1. Introduction

Cracking is commonly observed in concrete structures. Thus, understanding all types of cracking is important; cracking is due to different causes and may have different effects on short- and long-term performances because of the confounding effects of design, imposed loads, and climatic conditions relevant to the structure [1]. The many types of concrete cracking can be divided into two major categories, namely, micro-cracking and macro-cracking [2].

Currently, two types of testing methods are used in detecting and monitoring the deterioration in concrete structure: destructive testing (DT) and non-destructive testing (NDT). These methods are based on different principles and have different effectiveness on different types of deterioration. The acoustic emission (AE) technique is considered as one of the most promising techniques from various types of NDT methods [3]. The AE method and other NDT methods differ in two main features. First, in AE, the energy signal originates from the sample itself making its own signal, in response to stress. Second, the AE can detect the dynamic process because of its capability to detect movement or strain, whereas most of the other methods have the ability to detect existing geometrical discontinuities or fractures [4]. Thus, AE techniques have been applied to detect the crack location [5,6], to quantify the degree of damage [7–9], and to determine the crack classification [10–12] in concrete structures.

Crack patterns and propagations are mainly dependent on loading types and loading conditions. According to a recent study [5], the initial cracking position depends on the internal cracks and flaws during the loading, and the mechanical behavior of

* Corresponding author. Address: School of Civil Engineering, Universiti Sains Malaysia, Engineering Campus, Nibong Tebal, 14300 Penang, Malaysia. Tel.: +60 4 5996259; fax: +60 4 5941009.
E-mail address: cenorazura@eng.usm.my (N. Muhamad Bunnori).

0950-0618/$ - see front matter © 2013 Elsevier Ltd. All rights reserved.
http://dx.doi.org/10.1016/j.conbuildmat.2013.03.090

reinforced concrete beams can be divided into five stages, namely, micro-cracking, first visible cracking, distributed flexural cracking, shear cracking, and damage localization. The damage localization stage occurs when the initial cracks propagate upward to the compression zone, and the cracks start to localize into major cracks where the width of each crack is significantly widened.

The most important phase is the correlation of the cracking mode to the AE indices [11,13]. In most types of RC structure when load is applied, shear cracks develop after the formation of tensile cracks [11,14]. Two classification methods can be used to identify the fracture mechanisms and cracks classification in the RC structure by using AE. These methods are the moment tensor analysis (MTA) of AE signal-based method and the AE parameter analysis-based method, which is based on the JCMS-III B5706 code [10,11,15].

The AE parameters are influenced by the type of loading [16–19], maximum aggregate size (d_{max}) [20], and material characteristics [12,21,22]. Moreover, the AE technique has been applied to different volumes of concrete specimens under compression, such as cube and slender specimens [23]. However, the effect of varying structure sizes on the AE output data, such as RC with varying thicknesses, have not yet been studied fully.

In this study, 12 RC beams with different thicknesses were prepared and tested under the four-point bending test associated with AE equipment. The present paper is a complementary to previous paper [24]. Where, the main objectives of the present paper are to examine the behavior of cracks at each stage of the mechanical behavior of the RC beams from loading to failure using AE parameter analysis-based method, which had not been investigated in the previous paper. Moreover, this paper also attempts to examine the effect of the changes in the thickness of beam and level of damage on the parameters (RA and A-FRQ) of the AE parameter analysis-based method, noticing that RA parameter had not been investigated in the previous paper. Furthermore, this paper also aims to classify the crack types of RC beams with varying thicknesses based on the fracture mechanism of the RC beams and the acoustic emission signal features. Finally, this paper attempts to indicate the ratios of flexural and shear cracks at each level of damage for all beam types, which had not been investigated in the previous paper.

2. Crack classification based on AE parameters

2.1. AE parameter analysis

The AE parameter with correlation to the mode of cracks, or the Average Frequency (A-FRQ), and the RA value shown in Fig. 1 are used to classify the active cracks [13,15]. The A-FRQ is derived from the AE features of AE counts and duration, whereas the RA parameter value is the Rise Time (RT), which is defined as the delay between the onset and the maximum amplitude over the amplitude (A) [10–13].

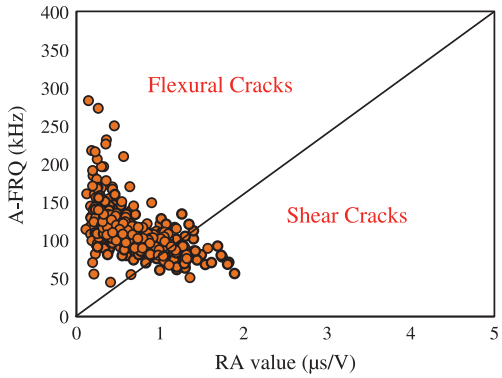

Fig. 1. Relationship between AF and RA value according to JCMS-III B5706 [15] and Ohno and Ohtsu [10].

$$\text{The average frequency} = \text{AE ringdown count}/\text{The duration time}, \quad (1)$$

$$\text{RA value} = \text{The rise time}/\text{The maximum amplitude}. \quad (2)$$

The behavior and properties of AE signal features during fracturing of the RC concrete sample under bending can be classified into two approaches according to the failure modes as shown in Table 1 and Fig. 2 [10–12].

3. Experimental procedure

3.1. Materials

The constituent materials include ordinary Portland cement (American Society for Testing and Materials [ASTM] Type 1, 42.5R), 14 days the cement was maintained in the site before experiment; natural river sand with a specific gravity of 2.7 and fineness modulus of 3.1; coarse aggregate with a maximum size of 20 mm with a specific gravity of 2.66 and steel reinforcement with a specified yield strength of 420 MPa.

3.2. Mix proportions and samples preparation

The proportions and properties of the normal concrete mix, according to American Standard ACI 318 code. These include a cement of 472 kg/m^3; natural river sand 797 kg/m^3; coarse aggregate 918 kg/m^3 and water/binder ratio of 0.446. The compressive strength was up to 47 MPa at 28 days and the slump was 120 mm.

Three types of RC beams with the same span length of 1500 mm and different thicknesses were prepared. All the beams were reinforced with high-yield 2Y10 and 2R8 diameter steel bars deformed at the tension and compression faces, respectively, according to American Standard ACI 318-08. The specimens were denoted by type, namely, Type I (TI), Type II (TII), and Type III (TIII), with stirrup center-to-center spacing of R6 diameter at 80, 100, and 130 mm, respectively. The difference between the three types is the beam thickness (H) as shown in Fig. 3. Where, the thickness of TI was 200 mm, TII was 250 mm and TIII was 300 mm. All beams were cured in water with a temperature of 27 ± 2 °C until testing day (after 28 days).

3.3. Loading and AE system

All the beams were tested under four-point loading (static stepwise monotonic loading) to examine the crack behaviors for all specimens and were monitored using the AE system. The first loading step was from 0.5 kN to 10 kN and was kept constant for 3 min prior to the next loading step until the failure stage. Four AE sensors (R6I) manufactured by Physical Acoustics Corporation with frequency ranges of 35–100 kHz were mounted on the specimen surface using magnetic clamps. The locations of the four sensors, namely, S1, S2, S3, and S4, are shown in Fig. 3. The threshold level was set at 45 dB to eliminate the electrical and mechanical noises [5].

In this study, the sampling rate was set to '1000kSPS' and the pre trigger setting were 250.000 μs, hit definition time (HDT) was 2000 μs, Wave velocity was 3500 m/s and lockout time (HLT) was 500 μs.

The full details about the experimental procedure in this paper have been presented in the previous paper [24].

Table 1
AE signal features behavior after crack propagation under bending [11–13].

AE signal features	Tensile mode	Shear mode
AE Waveform-length	Shorter	Longer
Rise time (RT)	Shorter	Longer
RA value	Decreased	Increased
Average frequency	Increased	Decreased
Realized energy – quantity	Smaller part	Larger
Realized energy – speed	More rapid	Slower

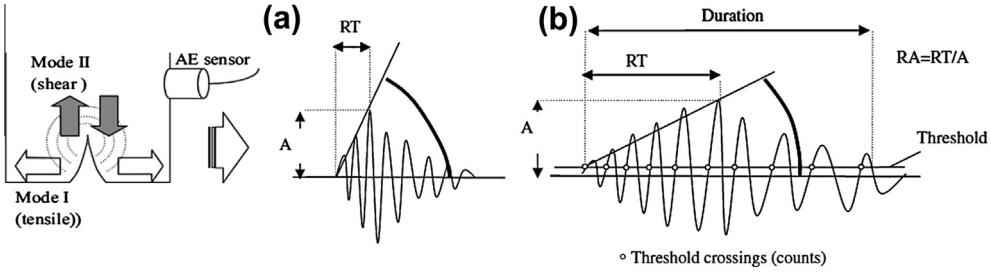

Fig. 2. Acoustic emission signal features: (a) tensile mode, and (b) shear mode [10–12].

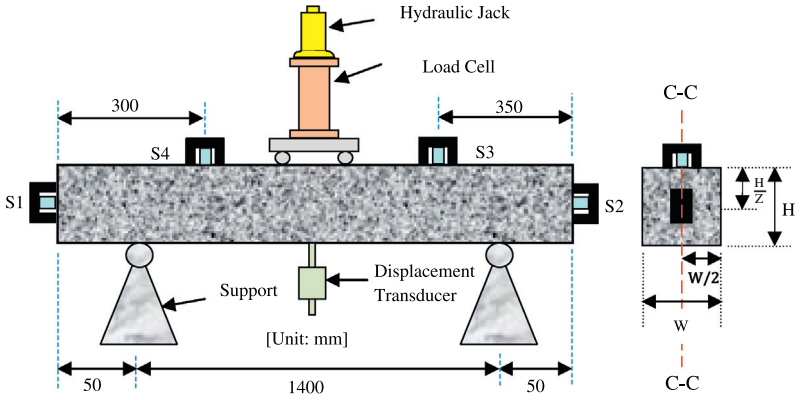

Fig. 3. Set-up of the four point bending test.

4. Test results and discussion

In the current study, the test results and subsequent discussion focused on all damage levels based on the fracture mechanism of the RC beams and AE activities.

4.1. Crack development (visual observation)

The crack pattern for any RC structure is mainly influenced by loading types and conditions. Generally, the initial cracking position depends on the internal cracks and flaws during loading [24,25]. Thus, the propagation of internal microcracks will lead to the first visual surface crack [5,17].

The crack developments and the mechanical behavior of these beams had been investigated visually by Aldahdooh et al. [25] at each level of damage. Where, they concluded that the majority of the cracks that propagated between the two point loads were flexural cracks for all beams. Moreover, the mechanical behavior of reinforced concrete beams can be divided into four different stages, namely, (I) micro-cracking, (II) appearance of first visible cracks (point A), (III) occurrence of distributed flexural and shear cracks (point B) and (IV) damage localization (point C). The load and corresponding displacement curve of one beam for each type (TI, TII, and TIII) are shown in Fig. 4. Moreover, Fig. 4 shows the load deflection curve of the three types of RC beams, where points A, B, and C reflect the values of loads at the first visible, distributed flexural, and mix-mode, as well as damage localization, respectively.

According to the final conclusion by Aldahdooh et al. [24], based on the visual observation for beam types, the failure mode at the earlier levels of damage until the appearance of the first visible cracks (before point B) occurred due to pure flexural cracks, whereas for the other levels of damage (after point B), the failure mode was unblemished with some shear cracks, but failure occurred for the majority of the flexure cracks for all beams as, shown in Figs. 5 and 6.

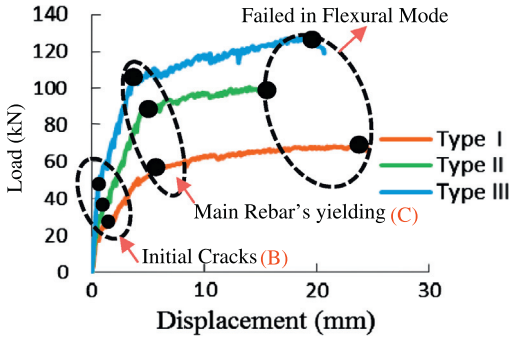

Fig. 4. Load–displacement of all beam types.

4.2. Crack classification by the modified AE parameter analysis method

Generally, in these types of beams, the first level of damage (micro-cracking) starts to generate initially accompanied by a number of recorded AE hits. The number of AE hits increases when the macroscopic cracks (first visible cracks and distributed flexural cracks) are formed. In this scenario, the maximum capacity or strength of the material is reached, and vertical displacement is largely observed. At the crack localization stage, the number of AE hits is lower than that in the previous stage and is related to the decrease in the cross-sectional area of the beam because of the increasing damage level up to the ultimate failure and because most of the cross section has been ruptured [11].

Findings based on visual observation and the principle of the AE parameter method indicate that the AE parameter method can be modified by analyzing the AE parameter at each level of damage

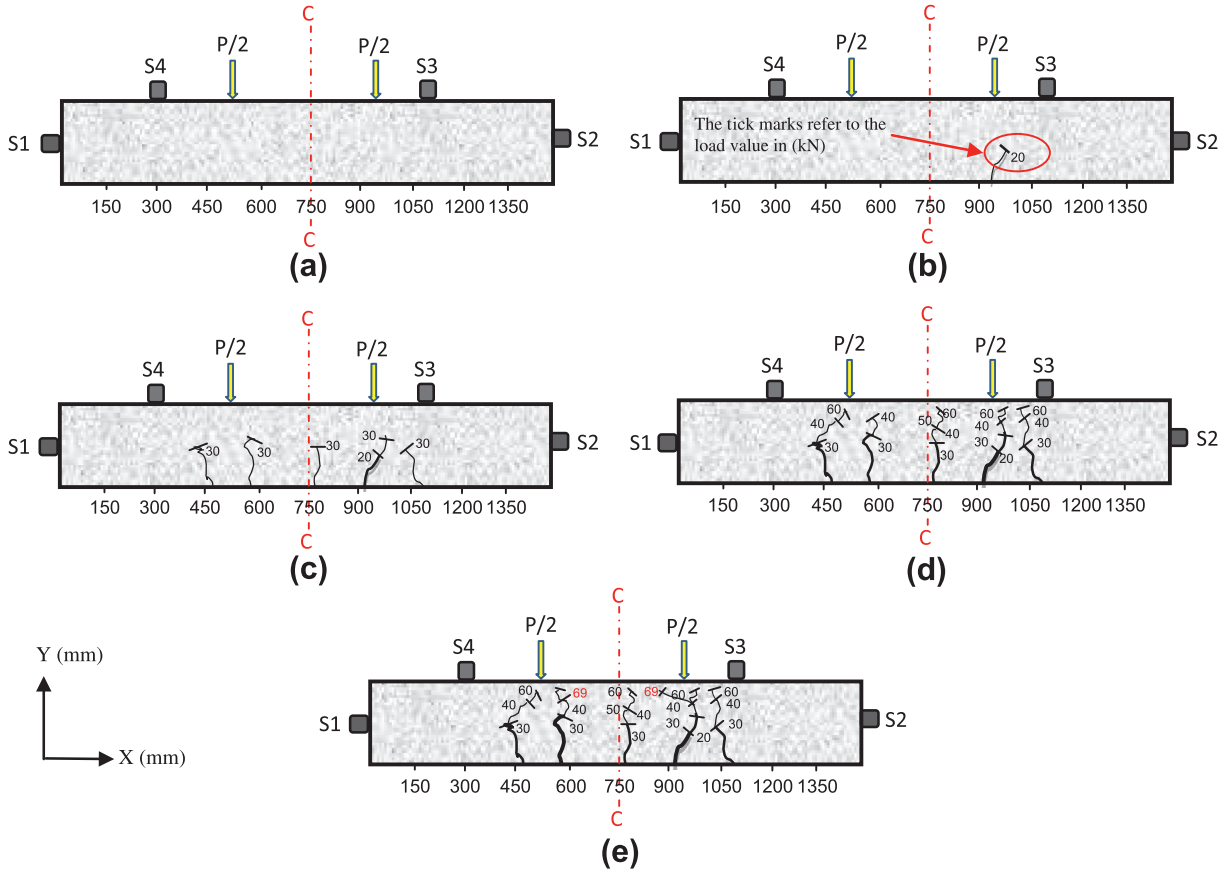

Fig. 5. Crack patterns obtained by visual observation of all category I: (a) stage I – as a micro-cracking, (b) stage II – as a first visible cracks, (c) stage III – as a distributed flexural cracks, (d) stage IV – as a damage localization, and (e) failure mode. (Load in kN, and distance in mm.)

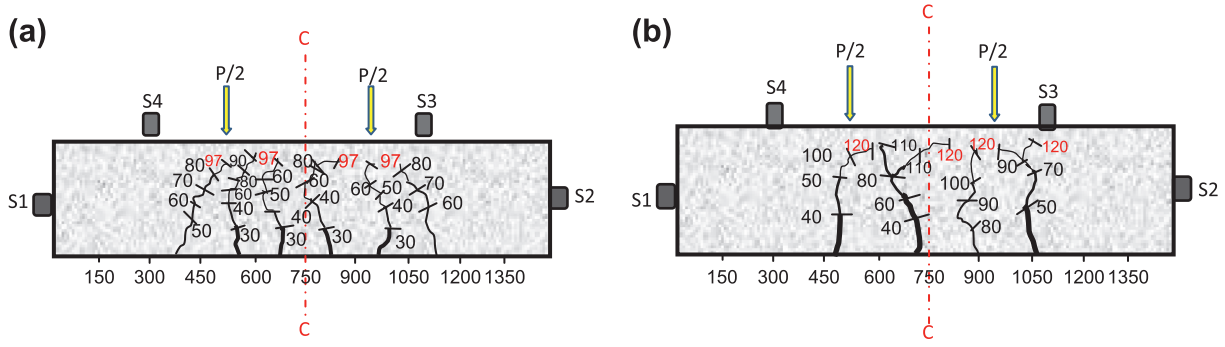

Fig. 6. Crack patterns obtained by visual observation at the final stage of damage: (a) TII, (b) TIII. (Load in kN, and distance in mm.)

to overcome the overlapping of the A-FRQ values among each level of damage as well as the RA values, as shown in Fig. 8. Where, Fig. 8 is very crowded with points that the reader cannot have a clear image and also it is too difficult to compare the values of the RA and A-FRQ between each levels. Modifying the AE parameter method will facilitate the classification process at each level of damage as shown in Fig. 7. Thus, when the majority of the RC structure is seen prior to failure, shear cracks appear to develop after tensile cracks [11,14].

Generally, parameter analysis is carried out by moving of the RA value and A-FRQ based on over 50 AE hits according to JCMS-III B5706 [15] and Ohno and Ohtsu [10] as shown in Fig. 1. In this case the proportion of RA and A-FRQ values were likewise set to 1:80 [10,15]. In the present paper, the AE signals for all beams were divided into four levels of damage according to the visual observation specified previously [24] to overcome the overlapping of the A-FRQ values among each level of damage as well as the RA values as shown in Fig. 7. The parameter analysis was undertaken by moving the average of the RA and A-FRQ values based on over 100 AE hits. The proportion of RA and A-FRQ values were likewise set to 1:80 according to JCMS-III B5706 [15] as stated by [10] as shown in Fig. 1.

Using the above modification, the third type of beams (TIII) was analyzed at each level of damage, as shown in Fig. 7. Fig. 8 shows the plots of A-FRQ vs. RA for all damage levels (I–IV) of TI, TII, and TIII.

Fig. 7 shows that the highest value of A-FRQ is always associated with the first level of damage. Moreover, the A-FRQ values

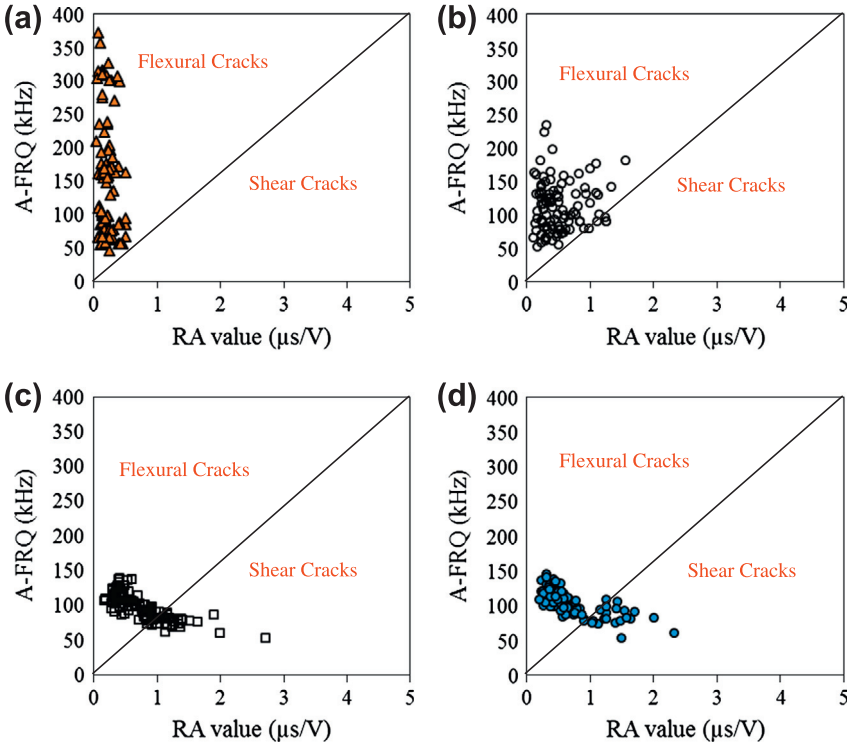

Fig. 7. Typical A-FRQ vs. RA for TIII beams: (a) damage level I, (b) damage level II (c) damage level III, and (d) damage level IV.

at the first level of damage (micro-cracking) were higher than those for the next damage stage. This behavior is related to the previous research conducted by [10,11,24]. The authors reported that flexural cracks usually develop at the initial stages of loading. Moreover, in the tensile mode, the value of the A-FRQ is always higher than its value in the shear mode [10–12], as shown in Table 1. Moreover, Fig. 7 shows no significant difference among the later stages of the damage, which had the lowest A-FRQ values due to the reduction in the cross-sectional area of the beam at the later stages of damage.

The above discussions were confirmed by the visual observation of the crack development at each level of damage specified in Section 4.1. The results showed that the failure mode at the earlier level of damage up to the first visible cracks occurred from pure flexural cracks, whereas for the other levels of damage, the failure mode was unblemished with shear cracks. However, failure occurred for the majority of flexure cracks for all beams, as shown in Figs. 5 and 6.

The highest A-FRQ values at the earlier stage of damage in TI were at 225 kHz, whereas those for TII and TIII were at 290 and 385 kHz, respectively, as shown in Fig. 8. The feasible interpretation of this result is that as the beam thickness increases, the crack length decreases, which in turn, results in an increased frequency of cracks [24]. This fact is compatible with the reduction in the cross-sectional area of the beam as increasing the damage level up to ultimate failure [11]. For example, if the load was applied to the three types of beams, namely, TI, TII, and TIII, with the same value and the crack length was measured at that load value, the shortest crack length will be associated with the beam with the largest thickness. The reduction in the cross-sectional area of the beam will decrease as the beam thickness increases, as shown in Figs. 5 and 6, and indicates that the lowest reduction is associated with largest beam thickness, which is the third type (TIII). Thus, the AE hit rate in the smallest thickness is lower than the largest thickness at each level.

The above discussion is compatible with the shear cracks phenomena, because the shear cracks (diagonal cracks) length always longer than the flexural cracks (vertical cracks) length. Where, the behavior is related to AE waveforms shape [24]. Since Kumar [26] reported that the waveforms shape is one of the most sensitive characteristic of the fracture mode. Hence, the value of the rise time parameter in the tensile mode crack is short, the average frequency value is high and RA value is low. Whilst in the shear mode crack type, result in longer waveforms, with longer rise time, lower average frequency and higher RA value [10–12]. This is mainly related on the transmitted energy quantity and speed. Where, there is an inverse relationship between the energy quantity and its speed. Hence, the energy speed at the later levels of damage (mix-mode cracks) is always slower than the earlier levels of damage (pure flexural cracks), this due to the larger part of energy transferred in the shear waves form; Therefore, the maximum peak of the waveform delays considerably compared to the onset of the initial longitudinal arrivals [11]. Accordingly, A-FRQ in the three types tends to increase as the thickness of the beams (200–300 mm) increased and RA value tends to decrease as the thicknesses increased, particularly at the earlier stages of damage.

Fig. 7 shows the RA parameter and indicates that the highest value of RA is always associated with the later stages of damage and that this behavior is related to the fact that the shear cracks is always associated with the later stages of damage. Moreover, the RA value in shear mode is always higher than its value in the tensile mode [10–12], which was described in Table 1.

Fig. 8 shows that the highest RA value is always associated with the smallest beam thickness T1 (20 cm), particularly at the earlier stage of damage. Figs. 7 and 8 show no significant difference among the later stages of damage (Level III and IV), which had the highest RA values. Fig. 9 shows the average RA values at each level of damage for all beam types, and indicates that the highest average RA values are always associated with the later levels of damage (III and IV), especially at the third level, which at this level

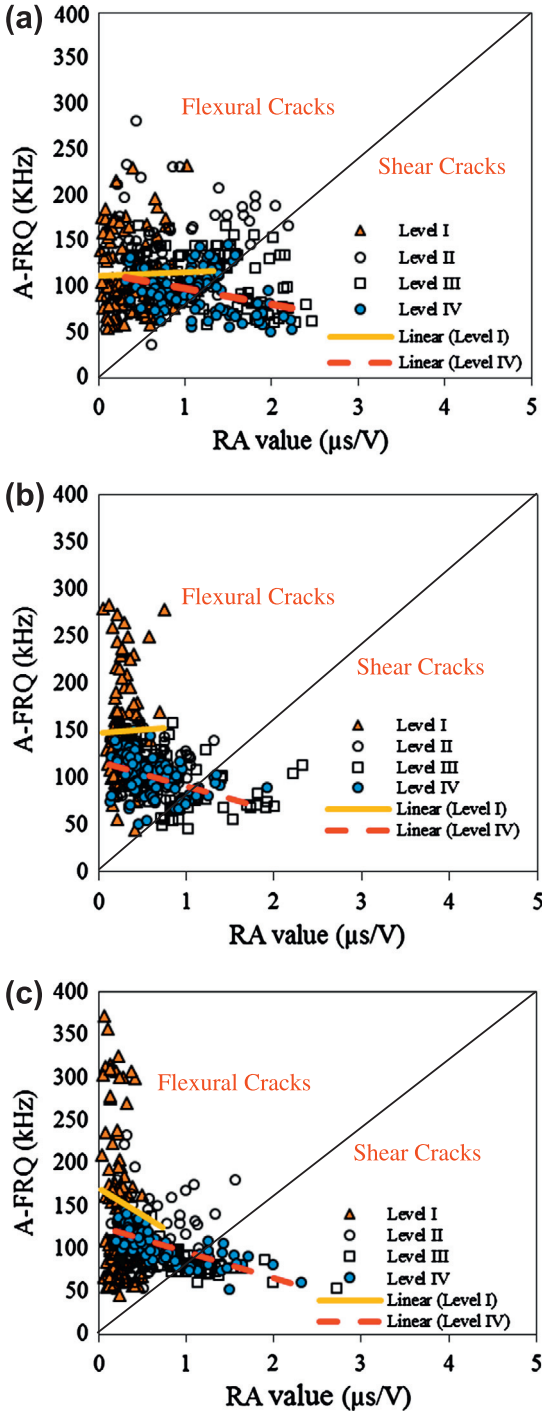

Fig. 8. Typical A-FRQ vs. RA for different damage levels: (a) TI beams; (b) TII beams and (c) TIII beams.

the shear cracks start to propagate. It is noticed from Fig. 9 that the RA value tend to slightly decrease in stage IV compared with stage III because and the cross section of beams at stage IV is almost ruptured. Moreover, the cracks mode at these stages (III and IV) can be considered as (mix-mode cracks), so the values seems quite same. Furthermore, the results indicated that the RA in the three types tends to decrease as the thickness of the beams (200–300 mm) increased, particularly at the earlier stages of damage (Figs. 7 to 9). The feasible interpretation of this result is that as the beam thickness increases, the crack length decreases, which in turn, results in

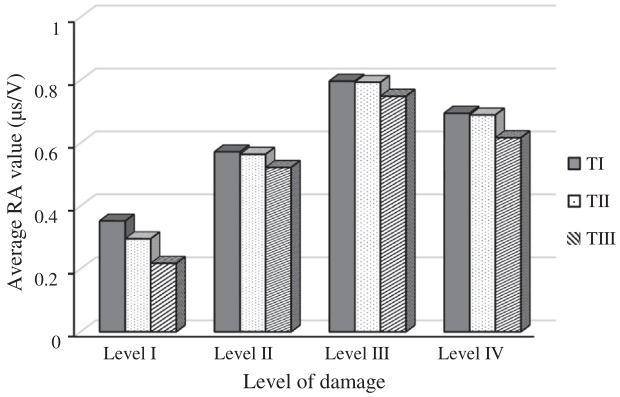

Fig. 9. Average RA value for TI, TII and TIII beams at each level of damage.

Table 2
Proportion of flexural and shear cracks at each level of damage for all types of beams.

Beams types						
	TI		TII		TIII	
Level of damage	Flexural cracks ratio (%)	Shear cracks ratio (%)	Flexural cracks ratio (%)	Shear cracks ratio (%)	Flexural cracks ratio (%)	Shear cracks ratio (%)
Level I	≈100	≈0	≈100	≈0	≈100	≈0
Level II	≈100	≈0	≈100	≈0	≈100	≈0
Level III	87.06	12.94	88.33	11.67	89.81	10.26
Level IV	82.90	17.10	85.25	14.50	87.95	12.35

an increased in the A-FRQ and a decrease in the RA value as discussed previously.

A comparison between visual observation and the modified AE parameter method to determine the shear and flexural ratios showed that all the cracks at the earlier stages of damage (I and II) were pure flexural cracks, whereas those that occurred at the latter stages of damage (III and IV) were mix-mode cracks, as shown in Figs. 5 and 8. Even so, the failure occurred in the majority of the flexure cracks for all beams at all damage levels. The ratios for shear cracks and flexural cracks at each level for all beams are described in Table 2.

Table 2 shows that the ratio of shear cracks at the failure stage becomes 17.10% of the AE hits and that 82.9% of AE hits are classified as tensile cracks for the 20 cm beam thickness (TI). On the other hand, for the 25 cm beam thickness (TII), the ratio of tensile crack was 85.25%, and 14.50% of the AE hits were classified as shear crack. For the 30 cm beam thickness (TIII), the ratio of shear cracks was 12.05% of AE hits, and 87.95% of the AE hits were classified as tensile cracks. These results coincided with the visual observation results according to crack development at each level of damage as specified in Section 4.1. Moreover, the ratios of the tensile cracks and shear cracks by parameter analysis are agreement with [10].

5. Conclusions

The following conclusions were reached based on the AE signal strength analysis as presented in this paper:

1. The visual observation showed that the failure occurred in the majority of flexure cracks for all beams at all levels of damage, particularly at the earlier stages of damage (micro-cracking and the first visible cracks stages).

2. Analyzing the AE data at each level of damage can help to overcome the overlap among levels and to classify the crack mode types and to indicate the ratios of flexural and shear cracks at each level of damage.
3. A comparison between visual observation and the modified AE parameter method to determine the shear and flexural ratios indicated that all the cracks that occurred at the earlier stages of damage (I and II) were pure flexural cracks, whereas the damages (III and IV) at the later stages were mix-mode cracks. Nevertheless, failure occurred in a majority of the flexure cracks for all beams at all damage levels.
4. The modified AE parameter method indicated the following:
    a. The A-FRQ and the RA values have an inverse relationship, especially at the earlier stages of damage, because the highest A-FRQ value is always associated with the first level of damage. Moreover, the A-FRQ value at any level of damage is higher than the A-FRQ value at the next stage.
    b. The highest A-FRQ value indicated at the earlier stages of damage for the 20 cm beam thickness was at 225 kHz, whereas those for 25 and 30 cm beam thicknesses were at 290 and 385 kHz, respectively.
    c. The highest RA value is always associated with the later stages of damage (III and IV). Moreover, the RA value tended to decrease at the earlier stages as the thickness of the beams (i.e., 200–300 mm) increased. The feasible interpretation of this result is that as the beam thickness increases for a given load, the crack length decreases, which in turn, results in an increased frequency and a decreased RA values of cracks.

The results showed that the AE technique is a promising technique for monitoring and classifying the failure modes of damage.

Acknowledgments

The authors wish to acknowledge the Universiti Sains Malaysia (USM) for providing the financial support through the USM fellowship scheme [APEX (1002/JHEA/ATSG/4001)], Short Term Grant (304/PAWAM/6039047) and Postgraduate Research Grant Scheme (1001/PAWAM/8045050).

References

[1] Yoon DJ, Weiss WJ, Shah SP. Assessing damage in corroded reinforced concrete using acoustic emission. J Eng Mech 2000;126(3):273–83.
[2] Kabir S, Rivard P, He DC, Thivierge P. Damage assessment for concrete structure using image processing techniques on acoustic borehole imagery. Constr Build Mater 2009;23(10):3166–74.
[3] Matsuyama K, Yamada M, Ohtsu M. On-site measurement of delamination and surface crack in concrete structure by visualized NDT. Constr Build Mater 2010;24(12):2381–7.
[4] Degala S. Acoustic emission monitoring of reinforced concrete systems retrofitted with CFRP [Master's Thesis]. University of Pittsburgh; 2008.
[5] Bunnori NM, Lark RJ, Holford KM. The use of acoustic emission for the early detection of cracking in concrete structures. Mag Concr Res 2011;63(9):683–8.
[6] Shiotani T, Shigeishi M, Ohtsu M. Acoustic emission characteristics of concrete-piles. Constr Build Mater 1999;13(1):73–85.
[7] Proverbio E. Evaluation of deterioration in reinforced concrete structures by AE technique. Mater Corros 2011;62(2):161–9.
[8] Degala S, Rizzo P, Ramanathan K, Harries KA. Acoustic emission monitoring of CFRP reinforced concrete slabs. Constr Build Mater 2009;23(5):2016–26.
[9] Lovejoy SC. Acoustic emission testing of beams to simulate SHM of vintage reinforced concrete deck girder highway bridges. Struct Health Monit 2008;7(4):329.
[10] Ohno K, Ohtsu M. Crack classification in concrete based on acoustic emission. Constr Build Mater 2010;24(12):2339–46.
[11] Aggelis DG. Classification of cracking mode in concrete by acoustic emission parameters. Mech Res Commun 2011;38(3):153–7.
[12] Soulioti D, Barkoula N, Paipetis A, Matikas T, Shiotani T, Aggelis D. Acoustic emission behavior of steel fibre reinforced concrete under bending. Constr Build Mater 2009;23(12):3532–6.
[13] Elfergani HA, Pullin R, Holford KM. Damage assessment of corrosion in prestressed concrete by acoustic emission. Constr Build Mater 2013;40:925–33.
[14] Yuyama S, Li Z, Ito Y, Arazoe M. Quantitative analysis of fracture process in RC column foundation by moment tensor analysis of acoustic emission. Constr Build Mater 1999;13(1–2):87–97.
[15] JCMS-III B5706. Monitoring method for active cracks in concrete by acoustic emission. Japan: Federation of Construction Materials Industries; 2003.
[16] Lim M, Koo T. Acoustic emission from reinforced concrete beams. Mag Concr Res 1989;41(149):229–34.
[17] Yun HD, Choi WC, Seo SY. Acoustic emission activities and damage evaluation of reinforced concrete beams strengthened with CFRP sheets. NDT & E Int 2010;43(7):615–28.
[18] Ohtsu M, Uchida M, Okamoto T, Yuyama S. Damage assessment of reinforced concrete beams qualified by acoustic emission. ACI Struct J 2002;99(4).
[19] Henkel D, Wood J. Monitoring concrete reinforced with bonded surface plates by the acoustic emission method. NDT & E Int 1991;24(5):259–64.
[20] Chen B, Liu J. Investigation of effects of aggregate size on the fracture behavior of high performance concrete by acoustic emission. Constr Build Mater 2007;21(8):1696–701.
[21] Aggelis D, Soulioti D, Barkoula N, Paipetis A, Matikas T. Influence of fiber chemical coating on the acoustic emission behavior of steel fiber reinforced concrete. Cem Concr Compos 2011;34(1):62–7.
[22] Chen B, Liu J. Damage in carbon fiber-reinforced concrete, monitored by both electrical resistance measurement and acoustic emission analysis. Constr Build Mater 2008;22(11):2196–201.
[23] Carpinteri A, Lacidogna G, Pugno N. Structural damage diagnosis and life-time assessment by acoustic emission monitoring. Eng Fract Mech 2007;74(1):273–89.
[24] Aldahdooh MAA, Muhamad Bunnori N, Megat Johari MAM. Damage evaluation of reinforced concrete beams with varying thickness using the acoustic emission technique. Constr Build Mater 2012.
[25] Aldahdooh MAA, Muhamad Bunnori N, Megat Johari MAM. Damage assessment of reinforced concrete beams at different flexural damage levels using acoustic emission technique. Malaysian Constr Res J 2013:1–13.
[26] Kumar A, Gupta A. Acoustic emission in fiber reinforced concrete. Exp Mech 1996;36(3):258–61.